


**Intense high-order harmonic generation in the giant fullerene molecule C<sub>240</sub>**H. K. Avetissian , S. Sukiasyan, T. M. Markosyan , and G. F. Mkrtchian \**Centre of Strong Fields Physics at Research Institute of Physics, Yerevan State University, Yerevan 0025, Armenia* (Received 4 October 2023; revised 1 December 2023; accepted 12 January 2024; published 1 February 2024)

In this work the extreme nonlinear optical response of the giant fullerene molecule C<sub>240</sub> in strong laser field is studied. The investigation of high-order harmonic generation in such quantum nanostructure is presented modeling the C<sub>240</sub> molecule and its interaction with the laser field in the scope of the tight-binding mean-field approach. The electron-electron interaction is modeled by the parametrized Ohno potential, which takes into account long-range Coulomb interaction. The essential role of the many-body Coulomb interaction in determining harmonic intensities is demonstrated. We also consider vacancy-defected molecule C<sub>240</sub>. The presence of a single vacancy breaks the icosahedral symmetry leading to the emergence of intense even-order harmonics. We examine the dependence of moderate harmonics on laser frequency that shows the multiphoton resonant nature of high harmonics generation. The dependence of cutoff harmonics on both laser intensity and frequency is examined too.

DOI: [10.1103/PhysRevB.109.085401](https://doi.org/10.1103/PhysRevB.109.085401)**I. INTRODUCTION**

Intense light interaction with nanostructures can excite the electrons of the system through multiphoton channels, leading to extreme nonequilibrium states [1]. The excited electrons subsequently emit coherent electromagnetic radiation, encompassing tens to hundreds of harmonics of the incident light [2,3]. This fundamental process in intense laser-matter interaction is known as the high harmonic generation (HHG) phenomenon [4,5]. In atoms, HHG has been widely used to produce coherent extreme ultraviolet radiation, allowing access to the extreme time resolution of the underlying quantum processes and enabling attosecond physics [6,7]. Among the diverse range of nanostructured materials suitable for nonlinear extreme optical applications, carbon allotropes hold a central position [8,9]. One of the carbon allotropes is fullerenes [10], which are large molecules formed by closing a graphite sheet, where the required curvature is achieved by incorporating twelve pentagons among a given number of graphene hexagons. The most well-known fullerene is the buckminsterfullerene C<sub>60</sub> [11], which possesses icosahedral symmetry. The discovery of fullerene C<sub>60</sub> through laser evaporation of graphite has triggered the study of many other fullerene molecules. Larger fullerenes, often referred to as giant fullerenes, can also be constructed with icosahedral symmetry [12]. These large fullerenes can be visualized as cut-out pieces of graphene that are folded into an icosahedron. Consequently, they exhibit similar properties to graphene [13] or graphene quantum dots [14], while remaining stable due to their closed topological structure. Note that in a continuous limit C<sub>60</sub> and related molecules are well described by the Dirac equation in the curved space and in the field of a monopole [15,16]. Giant or large fullerenes have been the

subject of active research since the 1990s. For a more comprehensive overview, we refer the reader to Refs. [17–23] for earlier studies and Refs. [24–30] for more recent investigations.

In the field of HHG, enhancing conversion efficiency is of utmost importance. This efficiency strongly relies on the density of emitters and the density of states of these emitters. To this end, molecular systems, clusters, and crystals have shown potential in significantly increasing harmonic intensity compared to atomic systems, as they can exploit multiple excitation channels [31–33]. As a result, there has been a growing interest in extending HHG to carbon-based materials, such as semimetallic graphene [34–50], graphene quantum dots [51–54], and fullerenes [55–66]. Experimental studies, namely Refs. [59,60], have reported a robust harmonic signal from C<sub>60</sub> plasma. Additionally, theoretical works have predicted strong HHG from both C<sub>60</sub> [56,57,65,66] and C<sub>70</sub> molecules [65] and solid C<sub>60</sub> [64]. Notably, the increase in conducting electrons in fullerene molecules leads to a subsequent rise in density of states, thereby opening up new channels that can amplify the HHG signal. Consequently, exploring the HHG process in giant fullerenes becomes a compelling area of interest. With the increasing fullerene size, the molecules are subject to various types of defects. Therefore, investigating the impact of defects on HHG in large fullerenes holds significance. Recent research involves effects of disorder, impurities, and vacancies on HHG in solids [67–75]. These studies have revealed that an imperfect lattice can enhance HHG compared to a perfect lattice, especially when considering doping-type impurities or disorders. For C<sub>60</sub> and C<sub>180</sub>, it has been shown that both diagonal and off-diagonal disorders break inversion symmetry, lift the degeneracy of states, and create new channels for interband transitions, resulting in enhanced high harmonic emission [66]. This raises intriguing questions about how vacancies specifically affect the HHG spectra in large fullerenes.

\*mkrтчian@ysu.am

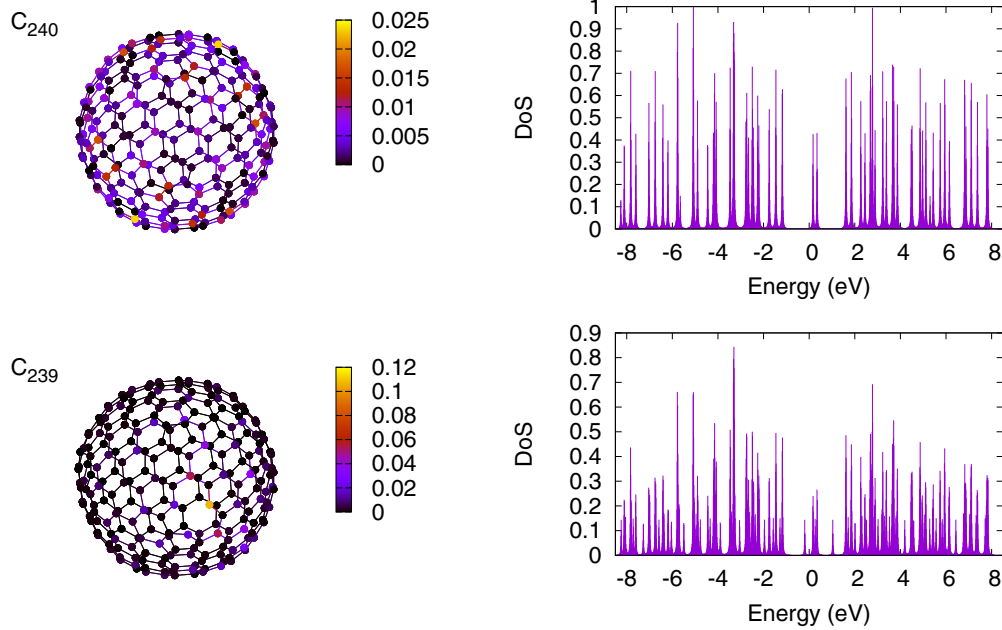


FIG. 1. The top and bottom panels represent  $C_{240}$  fullerene and  $C_{240}$  with a monovacancy, respectively. For brevity for refer to the latter as  $C_{239}$ . Within each row, the following visualizations are presented from left to right: electron probability density corresponding to the highest energy level in the valence band on the 3D color mapped molecular structures and the density of states. In DoS (arbitrary units) the Dirac delta function is approximated by a narrow Gaussian function. The obtained results are then normalized to the maximum value of the DoS for  $C_{240}$ .

Vacancies can occur naturally or be introduced in fullerenes through laser or ion/electron irradiation [76,77]. Taking into account that vacancy defects introduce localized electronic states [78] and the HHG process is highly sensitive to electron wave functions, we can expect new effects in the HHG process at consideration of vacancy-defected fullerenes.

In this study, we present a microscopic theory that explores the extreme nonlinear interaction of normal and single-vacancy-defected fullerene  $C_{240}$  with strong electromagnetic radiation. Particularly, we consider coherent interaction with a linearly polarized electromagnetic radiation taking into account collective electron-electron interactions. Employing the dynamical Hartree-Fock approximation, we reveal the general and basal structure of the HHG spectrum and its relation to molecular excitations and icosahedral symmetry breaking of giant molecules.

The paper is organized as follows. In Sec. II, the model and the basic equations are formulated. In Sec. III, we present the main results. Finally, conclusions are given in Sec. IV.

## II. THE MODEL AND THEORETICAL APPROACH

We start by describing the model and theoretical approach. Fullerene molecule  $C_{240}$  and  $C_{240}$  with a monovacancy are assumed to interact with a midinfrared or visible laser pulse that excites electron coherent dynamics. For brevity we refer to the vacancy-defected  $C_{240}$  molecule as  $C_{239}$ . The schematic structure of these fullerene molecules is deployed in Fig. 1. We assume a neutral molecule, which will be described in the scope of the tight-binding (TB) theory. The electron-electron interaction (EEI) is described in the extended Hubbard

approximation [65,79,80]. Hence, the total Hamiltonian reads

$$\hat{H} = \hat{H}_0 + \hat{H}_{\text{int}}, \quad (1)$$

where

$$\begin{aligned} \hat{H}_0 = & \sum_{i,\sigma} \mathcal{E}_0 c_{i\sigma}^\dagger c_{i\sigma} - \sum_{\langle i,j \rangle \sigma} t_{ij} c_{i\sigma}^\dagger c_{j\sigma} \\ & + \frac{U}{2} \sum_{i\sigma} n_{i\sigma} n_{i\bar{\sigma}} + \frac{1}{2} \sum_{i,j} V_{ij} n_i n_j \end{aligned} \quad (2)$$

is the free fullerene Hamiltonian. Here  $c_{i\sigma}^\dagger$  creates an electron with spin polarization  $\sigma = \{\uparrow, \downarrow\}$  at site  $i$  ( $\bar{\sigma}$  is the opposite to  $\sigma$  spin polarization), and  $\langle i, j \rangle$  runs over all the first nearest-neighbor hopping sites with the hopping integral  $t_{ij}$  between the nearest-neighbor atoms at positions  $\mathbf{r}_i$  and  $\mathbf{r}_j$ . The quantity  $\mathcal{E}_0$  is the average energy of the nonhybridized carbon orbitals [81]. The density operator is  $n_{i\sigma} = c_{i\sigma}^\dagger c_{i\sigma}$ , and the total electron density for the site  $i$  is  $n_i = n_{i\uparrow} + n_{i\downarrow}$ . The second and third terms in Eq. (2) describe the EEI Hamiltonian, with the parameters  $U$  and  $V_{ij}$  representing the on-site and the long-range Coulomb interactions, respectively. The involved molecules contain single and double carbon bonds, for which model Hamiltonian (2) has been parametrized extensively over the years. The input Cartesian coordinates for  $C_{240}$  are obtained from the Yoshida database [82]. In the present paper, as a first approximation, monovacancy is simulated by removing one carbon atom. The initial structures are further optimized with the help of the IQmol program [83]. Hence, in the vicinity of the vacancy the bond lengths are changed. There is also a scenario where the structure undergoes a bond reconstruction in the vicinity of the vacancy [84]. In either case, a local distortion of the lattice takes place resulting

in states that are strongly localized around defects [85,86]. For the one-electron hopping matrix elements, which in this work have been restricted to the nearest neighbors, we use values close to the graphene hopping matrix elements. The common choice of hopping matrix element is  $t_0 = 2.7$  eV, corresponding to the C-C bond length of  $d_0 = 1.42$  Å, while for shorter or longer bonds, its value is extrapolated using the linear relationship  $t_{ij} = t_0 + \alpha(d_0 - |\mathbf{r}_i - \mathbf{r}_j|)$ , with  $\alpha = 3.5$  eV/Å being the electron-phonon coupling constant. The EEI is modeled by the Ohno potential [87]:

$$V_{ij} = \frac{U}{\sqrt{1 + \frac{U^2 |\mathbf{r}_i - \mathbf{r}_j|^2}{V^2 d_m^2}}}, \quad (3)$$

where  $V$  means the strength of the long-range Coulomb interaction, and  $d_m$  is the average bond length. Depending on the screening effects a popular choice of parameters for the Coulomb interactions is  $0 \leq U \leq 4t_0$  and  $V = 0.5U$  [80,88].

The light-matter interaction is described in the length gauge

$$\hat{H}_{\text{int}} = e \sum_{i\sigma} \mathbf{r}_i \cdot \mathbf{E}(t) c_{i\sigma}^\dagger c_{i\sigma}, \quad (4)$$

where  $\mathbf{E}(t) = f(t)E_0\hat{\mathbf{e}} \cos \omega t$  is the electric field strength, with the amplitude  $E_0$ , frequency  $\omega$ , polarization  $\hat{\mathbf{e}}$  unit vector, and pulse envelope  $f(t) = \sin^2(\pi t/\mathcal{T})$ . The pulse duration  $\mathcal{T}$  is taken to be 10 wave cycles:  $\mathcal{T} = 20\pi/\omega$ . From the Heisenberg equation under the Hartree-Fock approximation one can obtain evolutionary equations for the single-particle density matrix  $\rho_{ij}^{(\sigma)} = \langle c_{j\sigma}^\dagger c_{i\sigma} \rangle$  [65]:

$$i\hbar \frac{\partial \rho_{ij}^{(\sigma)}}{\partial t} = \sum_k (\tau_{kj\sigma} \rho_{ik}^{(\sigma)} - \tau_{ik\sigma} \rho_{kj}^{(\sigma)}) + (V_{i\sigma} - V_{j\sigma}) \rho_{ij}^{(\sigma)} + e\mathbf{E}(t)(\mathbf{r}_i - \mathbf{r}_j) \rho_{ij}^{(\sigma)} - i\hbar\gamma(\rho_{ij}^{(\sigma)} - \rho_{0ij}^{(\sigma)}), \quad (5)$$

where  $V_{i\sigma}$  and  $\tau_{ij\sigma}$  are defined via density matrix  $\rho_{ij}^{(\sigma)}$  and its initial value:

$$V_{i\sigma} = \sum_{j\alpha} V_{ij}(\rho_{jj}^{(\alpha)} - \rho_{0jj}^{(\alpha)}) + U(\rho_{ii}^{(\sigma)} - \rho_{0ii}^{(\sigma)}), \quad (6)$$

$$\tau_{ij\sigma} = t_{ij} + V_{ij}(\rho_{ji}^{(\sigma)} - \rho_{0ji}^{(\sigma)}). \quad (7)$$

In addition, we assumed that the system relaxes at a rate  $\gamma$  to the equilibrium  $\rho_{0ij}^{(\sigma)}$  distribution. As we see, due to the mean field modification hopping integrals (7) become nonzero between the remote nodes, irrespective of the distance.

### III. RESULTS

Now we discuss full numerical solution of the evolutionary equations for the single-particle density matrix (5) and to get more physical insight, we study the question of which effects can be already observed in a linear regime of interaction. The time propagation of Eq. (5) is performed by the 8-order Runge-Kutta algorithm. As an initial density matrix we take a fully occupied valence band and a completely empty conduction band. To study the HHG process in the giant fullerene molecule we evaluate the high-harmonic spectrum by Fourier transformation of the dipole acceleration,

$\mathbf{a}(t) = d^2 \mathbf{d}(t)/dt^2$ , where the dipole momentum is defined as  $\mathbf{d}(t) = e \sum_{i\sigma} \mathbf{r}_i \rho_{ii}^{(\sigma)}(t)$ ,

$$\mathbf{a}(\Omega) = \int_0^{\mathcal{T}} \mathbf{a}(t) e^{i\Omega t} W(t) dt,$$

and  $W(t)$  is the window function to suppress small fluctuations [89] at the beginning and at the end of interaction to decrease the overall background (noise level) of the harmonic signal. We employ a hyper-Gaussian window function

$$W(t) = \exp\{-[a\omega(t - 0.5\mathcal{T})]^{16}\}$$

with constant  $a = 0.036$  to ensure a flat window throughout the entire interaction time. To capture a characteristic interaction dynamics that is independent of the molecule's orientation concerning laser polarization, we adopt the wave polarization unit vector as  $\hat{\mathbf{e}} = (1/\sqrt{3}, 1/\sqrt{3}, 1/\sqrt{3})$ , except for Fig. 11. For convenience, we normalize the dipole acceleration by the factor  $a_0 = e\bar{\omega}^2 \bar{d}$ , where  $\bar{\omega} = 1$  eV/ $\hbar$  and  $\bar{d} = 1$  Å. The power radiated at the given frequency is proportional to  $|\mathbf{a}(\Omega)|^2$ .

We begin by examining electronic structures of considered systems and the effect of vacancy on the states near the Fermi level. In Fig. 1, we illustrate electron probability density corresponding to the highest energy level in the valence band on the 3D color mapped molecular structures and density of states  $\text{DoS} = \sum_n \delta(\mathcal{E}_n - \mathcal{E})$  for considered molecules. For DoS  $\mathcal{E}_0$  is taken as the energetic reference. As is seen from this figure, for a vacancy-defected case we see the emergence of state near the Fermi level which is strongly localized around the vacancy. The DoS for  $\text{C}_{239}$  is somewhat suppressed, which is the result of breaking the icosahedral symmetry and lifting the degeneracy of states. To calculate the energies of the highest occupied molecular orbital (HOMO) and the lowest unoccupied molecular orbital (LUMO) we need  $\mathcal{E}_0$ . To establish a reference point, we define  $\mathcal{E}_0$  using  $\text{C}_{60}$  as a benchmark molecule, benefiting from its well-documented theoretical and experimental data. The first ionization energy  $I_p$  of neutral  $\text{C}_{60}$  has been estimated through electronic structure calculations, yielding a range of 7.35 to 9.1 eV [90–92]. Alternatively, an experimental value of  $I_p = 7.6$  eV is well established [93], which will be adopted in this paper. Using Koopman's theorem [94] and considering that the highest valence band TB level for  $\text{C}_{60}$  is  $\mathcal{E}_0 - 1.6$  eV, we can readily obtain  $\mathcal{E}_0 = -6$  eV. Thus, our calculations show that for the  $\text{C}_{240}$   $\mathcal{E}_{\text{HOMO}} = -7.2$  eV, and the LUMO is at  $\mathcal{E}_{\text{LUMO}} = -5.83$  eV. The HOMO-LUMO gap is 1.37 eV, which is in good agreement with data predicted in Refs. [95,96]. The next orbital where the dipole-allowed transition from HOMO is possible is at  $\mathcal{E}_{\text{LUMO}+1} = -5.65$  eV. For the  $\text{C}_{239}$  these parameters are  $\mathcal{E}_{\text{HOMO}} = -6.2$  eV,  $\mathcal{E}_{\text{LUMO}} = -5.83$  eV, and  $\mathcal{E}_{\text{LUMO}+1} = -5.65$  eV. That is, the first dipole-allowed transition gap for  $\text{C}_{239}$  is reduced. According to Koopman's theorem the ionization potential for both molecules can be estimated as  $-\mathcal{E}_{\text{HOMO}}$ . It is worth noting that at the TB level of theory, the results are independent of  $\mathcal{E}_0$ . However, for the validity of the obtained results, the pump field intensity should be kept sufficiently small to neglect ionization channels. Specifically, the ponderomotive energy  $U_p$  [97] for the considered laser fields must be much smaller than the ionization potential. In

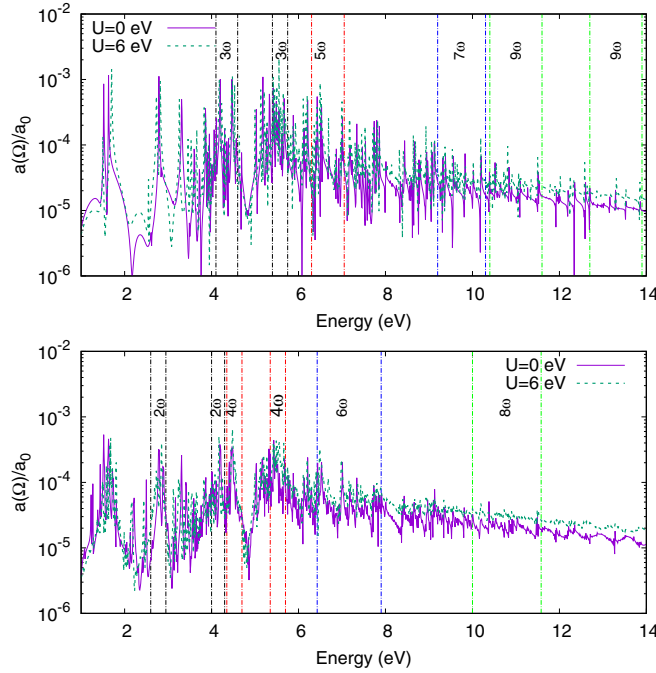


FIG. 2. The top and bottom panels represent  $C_{240}$  and  $C_{239}$ , respectively. We show intrinsic molecular excitations (linear absorption spectra) via the normalized dipole acceleration Fourier transformation (in arbitrary units), for Coulomb interaction turned on and off. The vertical dashed lines demarcate transitions responsible for  $n$ -photon resonant HHG, which will be considered regarding Figs. 5 and 6.

this paper, the maximal value of  $U_p$  is less than  $\hbar\omega$ , and  $\hbar\omega$  is significantly smaller than the ionization potential for the considered laser fields.

The intrinsic molecular excitations can be discerned through the frequency-dependent response function, which can be derived by solving the Casida equation, the Tamm-Dancoff equation, or the modified Sternheimer equation [98]. Alternatively, equivalent information can be extracted through the real-time propagation [98] using Eq. (5), provided the appropriate external electric field is employed. To achieve this, we consider an electric field with a sufficiently broad spectral shape to uniformly excite all electronic eigenmodes of the system. Hence we take

$$\mathbf{E}(t) = \hat{\mathbf{e}}E_0 \exp\{-\Delta^2(t - 0.5T)^2/4\} \quad (8)$$

with  $\Delta = 20$  eV/ $\hbar$ . The amplitude is chosen to be  $E_0 = 10^{-4}$  V/ $\text{\AA}$  to avoid nonlinear effects. Besides, the relaxation rate is taken to be very small  $\hbar\gamma = 0.5$  meV to resolve transitions as much as possible. In Fig. 2 we show molecular excitations (linear absorption spectra) via the dipole acceleration Fourier transformation  $a(\Omega)$  at the excitation with the field (8), for Coulomb interaction, turned on and off. The peaks are intrinsic molecular excitation lines and the area of a particular peak defines the weight of the oscillator strengths. The effects of the EEI are similar to those of the fullerene molecule  $C_{60}$  [80]. The Coulomb interaction shift peaks to higher energies, and oscillator strengths at higher energies have relatively larger weight than in the free electron

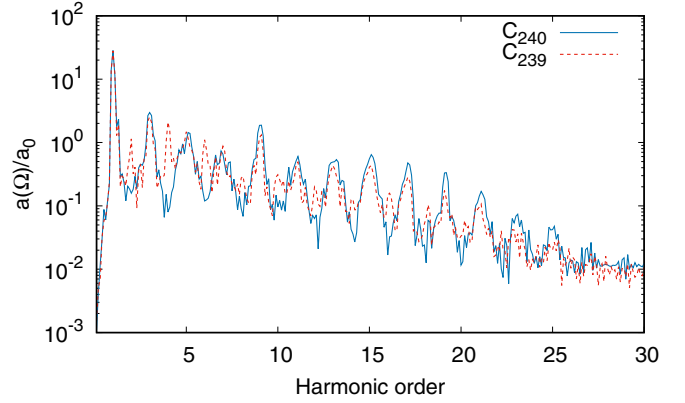


FIG. 3. The HHG spectra in the strong-field regime in logarithmic scale via the normalized dipole acceleration Fourier transformation  $a(\Omega)/a_0$  (in arbitrary units) for  $C_{240}$  and for  $C_{239}$ . The laser frequency is  $\omega = 1.2$  eV/ $\hbar$ . The spectra are shown for EEI energy  $U = 6$  eV.

case. These effects are due to the fact that the long-range Coulomb interactions (3) give rise to large hopping integrals between the remote nodes (7) in the Hartree-Fock approximation. For the vacancy-defected case the transitions are overall suppressed compared to the intrinsic case, although the low-energy transitions are strongly modified. From this figure we also see that the optical gap in fullerene molecule  $C_{240}$  is shifted to approximately 1.7 eV, which is narrower than that in  $C_{60}$  (2.8 eV). Notably, in both cases the absorption spectra exhibit many peaks up to the high energies, suggesting the presence of efficient multiphoton excitation channels and subsequent high-energy single-photon transitions. These factors play a significant role in shaping the HHG spectrum, as we will explore in the following.

Next, we will study more comprehensively the extreme nonlinear response of the giant fullerene molecule  $C_{240}$  and its vacancy-defected counterpart  $C_{239}$ . For all further calculations, except of Fig. 8, the relaxation rate is taken to be  $\hbar\gamma = 0.1$  eV. In Fig. 3, we show the typical HHG spectra in the strong-field regime ( $E_0 = 0.5$  V/ $\text{\AA}$ ) for both molecules. For the  $C_{240}$  molecule, the presence of inversion symmetry restricts the appearance of only odd harmonics in the HHG spectrum. In contrast, the introduction of a single vacancy in the  $C_{239}$  molecule disrupts its icosahedral symmetry, resulting in the prominent emergence of even-order harmonics with enhanced intensity. Besides, we see a strongly nonlinear picture, where the strength of the 9th harmonic surpasses that of the 5th and 7th harmonics. Additionally, a distinctive plateau spanning from the 11th to the 21st harmonics exhibits comparable strengths. Notably, for the  $C_{239}$  molecule, the harmonics near the cutoff display a slight suppression relative to the  $C_{240}$  one. This disparity is attributed to the differing effectiveness of excitation channels, which favors enhanced harmonics in the case of the  $C_{240}$  molecule (see Fig. 2).

Let us now consider the influence of the pump wave frequency on the HHG process within the energy range of  $\hbar\omega = 1-2$  eV. This analysis is presented in Fig. 4 which illustrates the frequency-dependent HHG spectra. Notably, we discern that the position of the cutoff harmonic  $N_{\text{cut}}$

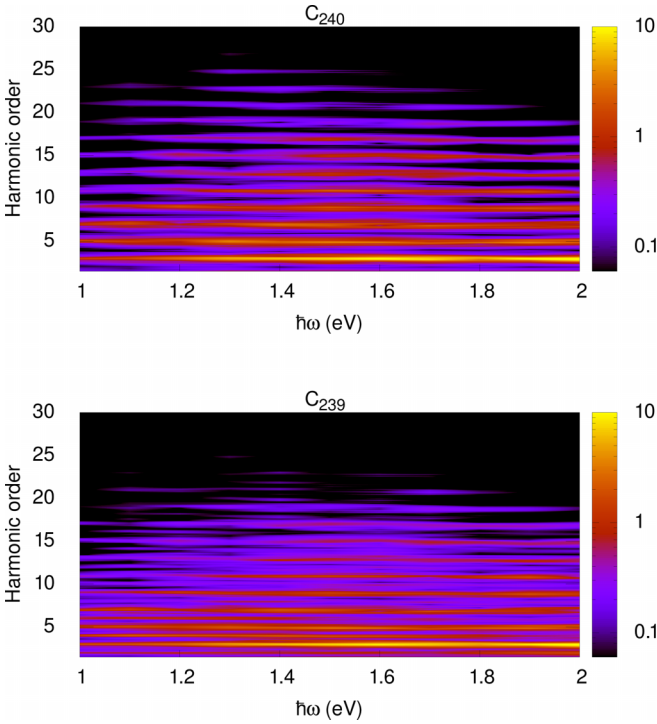


FIG. 4. The dependence of the HHG spectra on the wave field frequency is illustrated for  $C_{240}$  (top) and  $C_{239}$  (bottom) using the normalized dipole acceleration Fourier transformation,  $a(\Omega)/a_0$ , plotted on a logarithmic scale. The wave amplitude is taken to be  $E_0 = 0.5 \text{ V/\AA}$ . The relaxation rate is set to  $\hbar\gamma = 0.1 \text{ eV}$ . The EEI energy is  $U = 6 \text{ eV}$ .

demonstrates a relatively gradual response to changes in the wave field frequency  $\omega$ . Additionally, this cutoff exhibits distinctive peaks within the midfrequency range. It is worth noting that in atomic HHG processes involving free continua, the cutoff harmonic position  $N_{\text{cut}} \sim \omega^{-3}$  [5]. Furthermore, a noteworthy feature emerges when considering the  $C_{239}$  molecule: even-order harmonics are suppressed for higher frequency pump waves. This phenomenon can be attributed to the fact that with higher frequency pump waves, excitation and recombination channels predominantly involve highly excited states that still retain the inversion symmetry. Of particular interest is the plateau region within the spectra. Here, a pattern of alternating variation in relation to frequency becomes evident, a hallmark of multiphoton resonant transitions between the valence and conduction bands. This resonant behavior is further illuminated by Figs. 5 and 6, where we visualize the dependency of emission strength for the pre-plateau harmonics on the pump wave frequency. It is apparent that these harmonics exhibit resonant behavior. Upon a closer examination of Fig. 2, we discern that the molecular excitations exhibit peaks coinciding with these resonant frequencies, providing supplementary evidence for the multiphoton resonant transitions. For the considered frequencies,  $n$ -photon resonant transitions fall within the range  $\hbar\Delta_n \simeq (n \text{ eV}, 2n \text{ eV})$ . In Fig. 2, we delineate transitions responsible for  $n$ -photon resonant HHG, taking into account the widths of peaks in Figs. 5 and 6. It is important to note that the peak width  $\delta_n$  in Figs. 5 and 6 corresponds

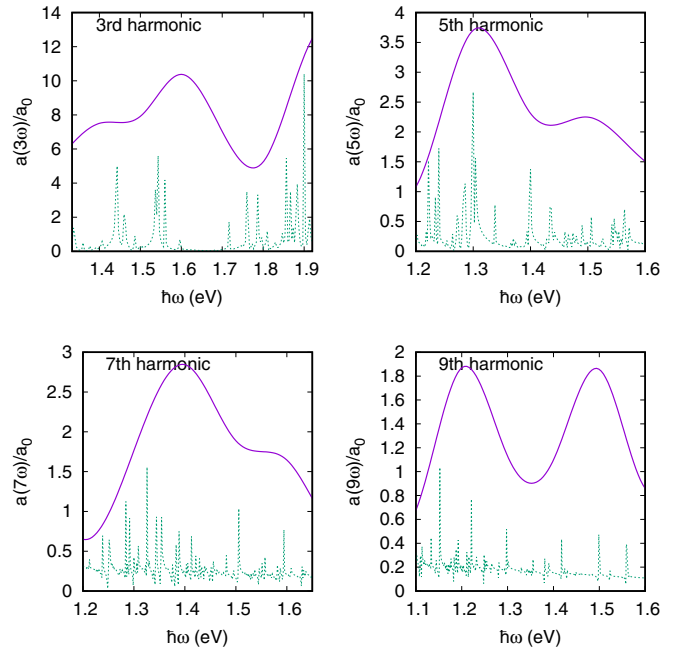


FIG. 5. The dependence of emission strength in the case of  $C_{240}$  for the 3rd, 5th, 7th, and 9th harmonics on the pump wave frequency for the setup of Fig. 4. Additionally, the linear absorption spectra  $a(\Omega/n)$  are depicted by dashed lines, where  $n$  denotes the harmonic order. The linear absorption spectra are appropriately scaled for visual clarity.

to  $n\delta_n$  in Fig. 2. Additionally, these peaks are expected to have widths on the order of the electron-wave interaction energy  $eE_0d_{\text{tr}}$ , where  $d_{\text{tr}}$  represents the typical transition dipole moment. Multiple transition channels can also contribute to spectral line broadening. To delineate the transitions

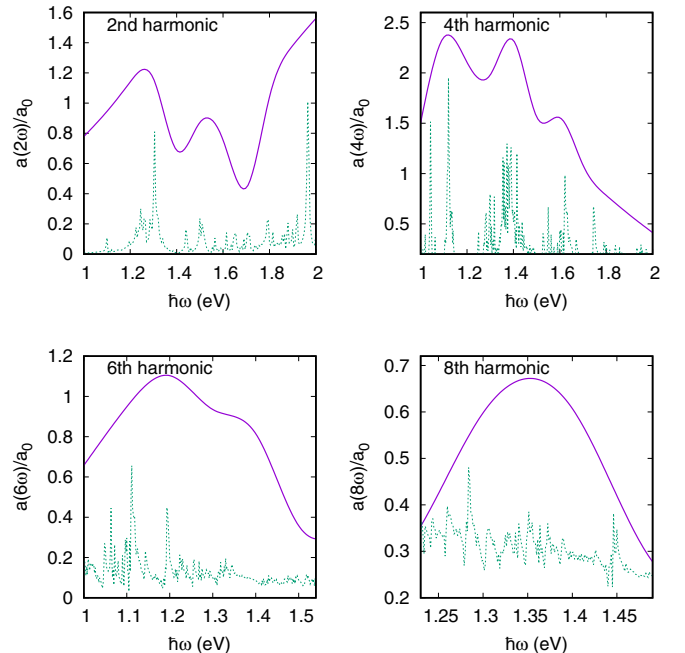


FIG. 6. Similar to Fig. 5, this figure illustrates the scenario for  $C_{239}$ , specifically focusing on the 2nd, 4th, 6th, and 8th harmonics.

responsible for  $n$ -photon resonant HHG in Fig. 2, the linear absorption spectra  $a(\Omega/n)$  are overlaid within Figs. 5 and 6, represented by dashed lines. For instance, in the case of  $C_{240}$ , the peaks corresponding to the 3rd harmonic emerge at approximately 1.6 eV and 1.9 eV with widths around 0.2 eV. The peaks in the linear spectrum align closely with these peaks in the HHG spectra and encompass multiple excitation channels. In Fig. 5, the peak for the 5th harmonic at approximately 1.3 eV corresponds well with a local peak in the linear spectrum, accompanied by multiple excitation channels. Similarly, for  $C_{239}$ , the peaks of the 2nd harmonic appear around 1.25 eV and 2.0 eV, with corresponding transitions in the linear spectrum. The peaks of the 4th harmonic also align with local peaks in the linear spectrum. This tendency extends to transitions for the 6th, 7th, 8th, and 9th harmonics.

The impact of multiphoton effects becomes significant when the characteristic electron-wave interaction energy  $eE_0d_{tr}$  becomes comparable to or exceeds the photon energy  $\hbar\omega$  of the pump wave. In this context the typical transition dipole moment can be estimated to be approximately  $d_{tr} \sim d_0$ . For our specific scenario, we specially choose pump wave frequency and electron-wave interaction energy to be considerably smaller than the ionization potential to avoid the involvement of other excitation channels that fall outside the scope of our approximate model. Nevertheless, with the given parameters, where  $eE_0d_{tr}/\hbar\omega \sim 0.5$ , the multiphoton excitation of unoccupied molecular orbitals becomes significant. In such cases, these multiphoton transitions can exhibit both resonant and nonresonant characteristics. It is crucial to note that unlike nonresonant transitions, the resonant transitions necessitate a substantial residual population of levels after the interaction is turned off. The multiphoton resonance-driven characteristics are further supported by the evident alteration in the population of energy levels within the valence and conduction bands, as highlighted in Fig. 7. Note that, for a chosen frequency, the transitions from HOMO to higher unoccupied molecular orbitals are possible through the multiphoton channels. This figure presents the post-interaction population distribution of energy levels, demonstrating a marked departure from the equilibrium distribution. This discrepancy underscores the substantial impact of multiphoton resonant transitions within the HHG process of giant fullerene  $C_{240}$  under the influence of intense near-infrared laser fields.

Continuing our exploration, let us examine the influence of the relaxation rate on the HHG phenomenon across a span of  $\hbar\gamma = 0.1-0.2$  eV. The corresponding dependencies of the HHG spectra on the relaxation rate are presented in Fig. 8. It is discernible that HHG exhibits resistance to relaxation processes, with pre-plateau harmonics, in particular, displaying notable robustness.

As have been seen from Fig. 2, the position of molecular excitonic lines and relative intensities depend on EEI. It is also expected that HHG yield changes due to EEI. The latter is shown in Fig. 9, where the HHG spectra in the strong-field regime for different EEI energies are shown for the fullerene  $C_{240}$  molecule. We have a similar picture for the  $C_{239}$  molecule. As is seen, HHG yield strongly depends on the EEI energy. The inclusion of the Coulomb interaction leads to two noteworthy characteristics in the HHG spectra: (a) The

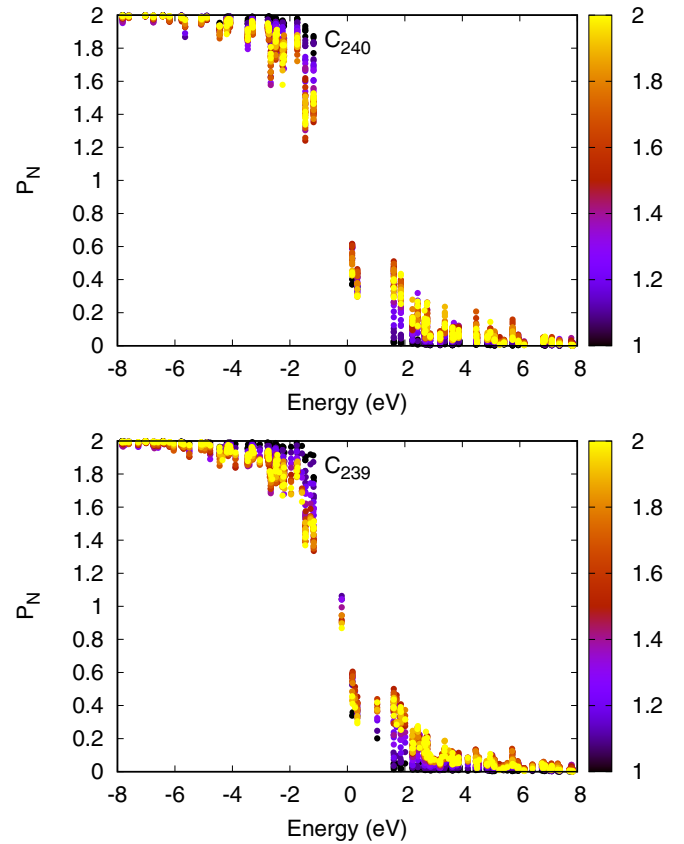


FIG. 7. The residual population of levels for the setup of Fig. 3.

most prominent feature is a substantial increase in the HHG signal by several orders of magnitude near the cutoff regime compared to the case of free quasiparticles. (b) The cutoff frequency is significantly enhanced. The substantial increase in the HHG signal can be elucidated by the mean-field modification of hopping integrals (7). The long-range nature of Coulomb interaction (3), coupled with the pronounced deviation of the single-particle density matrix from equilibrium in the intense laser field, causes the hopping integrals (7) to become significant even between the distant nodes, independent of the internode distance. Consequently, this enhancement in electron mobility leads to strong nonlinear oscillations of the dipole acceleration. This observation gains further support from the noticeable prominence of these features in the case of the giant fullerene  $C_{240}$ , in stark contrast to the behavior observed in the  $C_{60}$  molecule [65]. Another notable aspect of the HHG signals in giant fullerene molecules is their dependence on the size of the molecule. The HHG signals per particle for  $C_{240}$  and  $C_{60}$  are compared in Fig. 10. As demonstrated, there is a significant increase in the HHG signal for the  $C_{240}$  molecule, a result also observed for the  $C_{70}$  molecule according to previous studies [65]. This enhancement may be attributed to the density of states, which is indirectly reflected in Fig. 2 via the absorption spectra. The inset in Fig. 10 shows the linear absorption spectrum for the  $C_{60}$  molecule obtained in the same way, as in Fig. 2. This figure reveals that the  $C_{240}$  molecule has substantially more transition channels than the  $C_{60}$  one.

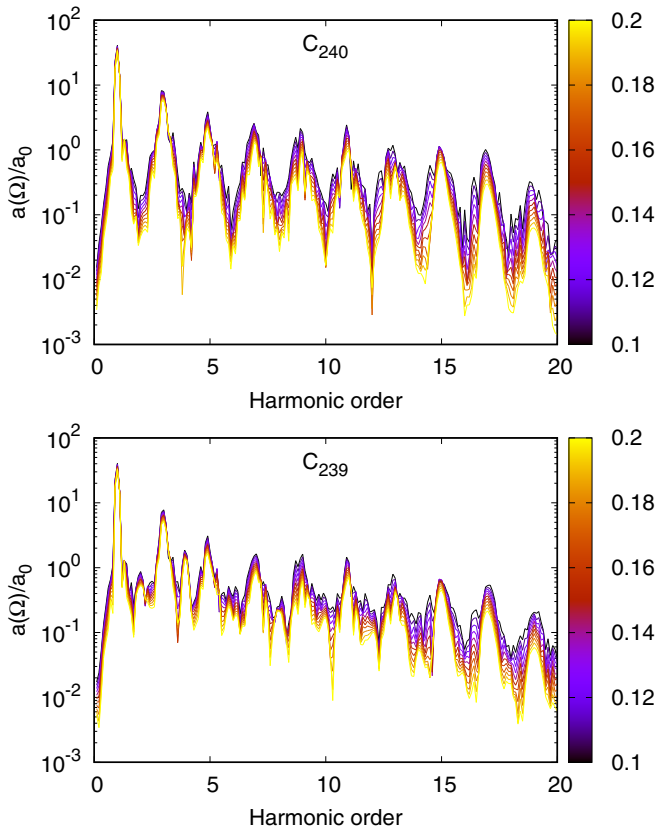


FIG. 8. The dependencies of the HHG spectra on the relaxation rate illustrated for  $C_{240}$  (top) and  $C_{239}$  (bottom). The spectra are shown for EEI energy:  $U = 6$  eV. The pump wave frequency is  $\omega = 1.5$  eV/ $\hbar$ . The wave amplitude is taken to be  $E_0 = 0.5$  V/Å. The color bar shows the relaxation rate in eV/ $\hbar$ .

Finally, note that within the scope of the described methodology we have explored the correlation between the cutoff frequency and the intensity of a pump wave by analyzing the HHG spectra for various intensities. The relationship between the HHG spectra and the amplitude of the wave field for both giant molecules is visually represented in Fig. 11. This figure prominently illustrates the nonlinear connection between the

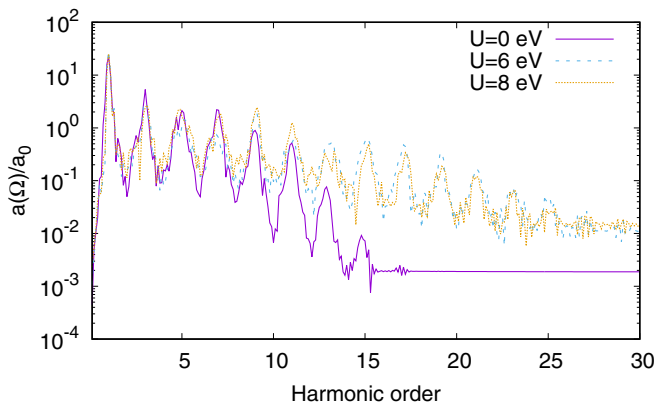


FIG. 9. The comparison of HHG signals for  $C_{240}$  at different EEI energies. The pump wave frequency is  $\omega = 1.2$  eV/ $\hbar$  and wave amplitude is  $E_0 = 0.5$  V/Å. The relaxation rate is set to  $\hbar\gamma = 0.1$  eV.

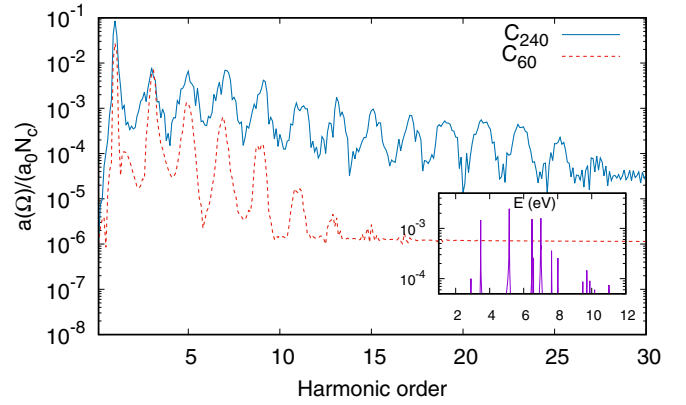


FIG. 10. The comparison of HHG signals per particle for  $C_{240}$  and  $C_{60}$ . The pump wave frequency is  $\omega = 1.1$  eV/ $\hbar$  and wave amplitude is  $E_0 = 0.5$  V/Å. The relaxation rate is set to  $\hbar\gamma = 0.1$  eV. The inset shows the linear absorption spectrum for  $C_{60}$  obtained in the same way as in Fig. 1.

pre-plateau harmonics and the amplitude of the pump wave. The analysis of the obtained results reveals that for high intensities, the positions of the cutoff harmonics can be adequately described by scaling with the square root of the field strength amplitude. The solid lines superimposed on the density plot in Fig. 11 represent envelopes ( $\sim\sqrt{E_0}$ ) that determine the positions of the cutoff harmonics. Notably, it is evident that these envelopes provide a reasonably accurate approximation for the cutoff harmonics for large field strengths. Note that the mechanism driving the HHG process in the considered

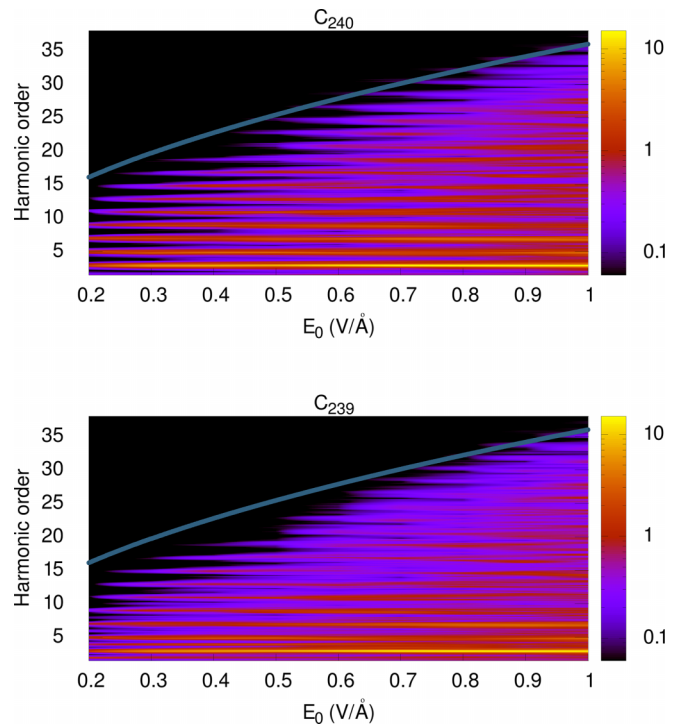


FIG. 11. The dependencies of the HHG spectra on the wave field amplitude are illustrated for  $C_{240}$  (top) and  $C_{239}$  (bottom) using the normalized dipole acceleration Fourier transformation,  $a(\Omega)/a_0$  (color bar), plotted on a logarithmic scale. The spectra are shown for EEI energy:  $U = 6$  eV. The pump wave frequency is  $\omega = 1.5$  eV/ $\hbar$ .

system noticeably differs from that in atomic systems, where the typical three-step model [5] is applicable, and the continuum serves as the energy accumulation site, yielding a cutoff energy proportional to the pump wave intensity. This departure from the established law is intrinsic to two-level systems [99,100] or nanostructures with pseudo-relativistic energy-momentum dispersion [101], wherein the cutoff energy scales linearly with the amplitude of the field strength. For giant fullerene molecules, we encounter a more complex scenario where an extensive array of energy levels significantly affects the HHG process through multiphoton resonances and level dressing. This complexity results in a more gradual increase in the cutoff energy with the rising intensity of the pump wave.

#### IV. CONCLUSION

We have done an extensive exploration of the highly nonlinear optical response of giant fullerene molecules, with a particular emphasis on  $C_{240}$ , which possesses the characteristic icosahedral point group symmetry often encountered in such molecular systems. To disclose the complete physical picture of the HHG process on giant fullerene molecules with the mentioned icosahedral symmetry, we have also

investigated a vacancy-defected molecule,  $C_{239}$ . Our investigation employed consistent quantum/analytic and numerical calculation of the HHG spectra using a mean-field methodology that rigorously accounts for long-range many-body Coulomb interactions too. Through the solution of the evolutionary equations governing the single-particle density matrix we have disclosed resonant effects within the HHG spectra and have demonstrated the fundamental role of Coulomb interaction in shaping the intensities of the harmonics. A significant enhancement in HHG yield, as compared with the fullerene molecule  $C_{60}$ , has been established. Moreover, our research has elucidated that the presence of a single vacancy, causing the breakdown of icosahedral symmetry, stimulates the appearance of pronounced even-order harmonics. In terms of the dependence of the cutoff harmonics on the intensity of the wave field, we have established that this relationship can be approximated with greater accuracy by scaling with the square root of the amplitude of a pump wave strength.

#### ACKNOWLEDGMENT

The work was supported by the Science Committee of the Republic of Armenia, Project No. 21AG-1C014.

- 
- [1] H. K. Avetissian, *Relativistic Nonlinear Electrodynamics: The QED Vacuum and Matter in Super-Strong Radiation Fields* (Springer, New York, 2015).
- [2] P. Agostini and L. F. DiMauro, The physics of attosecond light pulses, *Rep. Prog. Phys.* **67**, 813 (2004).
- [3] M. C. Kohler, T. Pfeifer, K. Z. Hatsagortsyan, and C. H. Keitel, Frontiers of atomic high-harmonic generation, *Adv. At. Mol. Opt. Phys.* **61**, 159 (2012).
- [4] P. B. Corkum, Plasma perspective on strong field multiphoton ionization, *Phys. Rev. Lett.* **71**, 1994 (1993).
- [5] M. Lewenstein, P. Balcou, M. Y. Ivanov, A. L'Huillier, and P. B. Corkum, Theory of high-harmonic generation by low-frequency laser fields, *Phys. Rev. A* **49**, 2117 (1994).
- [6] P. B. Corkum and F. Krausz, Attosecond science, *Nat. Phys.* **3**, 381 (2007).
- [7] F. Krausz and M. Ivanov, Attosecond physics, *Rev. Mod. Phys.* **81**, 163 (2009).
- [8] E. H. Falcao and F. Wudl, Carbon allotropes: Beyond graphite and diamond, *J. Chem. Technol. Biotechnol.* **82**, 524 (2007).
- [9] S. K. Tiwari, V. Kumar, A. Huczko, R. Oraon, A. D. Adhikari, and G. Nayak, Magical allotropes of carbon: Prospects and applications, *Crit. Rev. Solid State Mater. Sci.* **41**, 257 (2016).
- [10] R. E. Smalley, Discovering the fullerenes, *Rev. Mod. Phys.* **69**, 723 (1997).
- [11] H. W. Kroto, J. R. Heath, S. C. O'Brien, R. F. Curl, and R. E. Smalley,  $C_{60}$ : Buckminsterfullerene, *Nature (London)* **318**, 162 (1985).
- [12] H. Kroto and K. McKay, The formation of quasi-icosahedral spiral shell carbon particles, *Nature (London)* **331**, 328 (1988).
- [13] A. K. Geim, Graphene: Status and prospects, *Science* **324**, 1530 (2009).
- [14] A. D. Güçlü, P. Potasz, M. Korkusinski, and P. Hawrylak, *Graphene Quantum Dots* (Springer, Berlin, 2014).
- [15] J. Gonzalez, F. Guinea, and M. A. Vozmediano, The electronic spectrum of fullerenes from the Dirac equation, *Nucl. Phys. B* **406**, 771 (1993).
- [16] J. González, F. Guinea, and M. A. H. Vozmediano, Continuum approximation to fullerene molecules, *Phys. Rev. Lett.* **69**, 172 (1992).
- [17] D. York, J. P. Lu, and W. Yang, Density-functional calculations of the structure and stability of  $C_{240}$ , *Phys. Rev. B* **49**, 8526 (1994).
- [18] G. E. Scuseria, The equilibrium structures of giant fullerenes: Faceted or spherical shape? An *ab initio* Hartree-Fock study of icosahedral  $C_{240}$  and  $C_{540}$ , *Chem. Phys. Lett.* **243**, 193 (1995).
- [19] G. E. Scuseria, *Ab initio* calculations of fullerenes, *Science* **271**, 942 (1996).
- [20] S. Itoh, P. Ordejón, D. A. Drabold, and R. M. Martin, Structure and energetics of giant fullerenes: An order- $N$  molecular-dynamics study, *Phys. Rev. B* **53**, 2132 (1996).
- [21] C. H. Xu and G. E. Scuseria, An  $O(N)$  tight-binding study of carbon clusters up to  $C_{8640}$ : The geometrical shape of the giant icosahedral fullerenes, *Chem. Phys. Lett.* **262**, 219 (1996).
- [22] R. C. Haddon, G. E. Scuseria, and R. E. Smalley,  $C_{240}$ —The most chemically inert fullerene? *Chem. Phys. Lett.* **272**, 38 (1997).
- [23] M. I. Heggie, M. Terrones, B. R. Eggen, G. Jungnickel, R. Jones, C. D. Latham, P. R. Briddon, and H. Terrones, Quantitative density-functional study of nested fullerenes, *Phys. Rev. B* **57**, 13339 (1998).
- [24] B. I. Dunlap and R. R. Zope, Efficient quantum-chemical geometry optimization and the structure of large icosahedral fullerenes, *Chem. Phys. Lett.* **422**, 451 (2006).
- [25] R. R. Zope, T. Baruah, M. R. Pederson, and B. I. Dunlap, Static dielectric response of icosahedral fullerenes from  $C_{60}$



- to  $C_{2160}$  characterized by an all-electron density functional theory, *Phys. Rev. B* **77**, 115452 (2008).
- [26] P. Calaminici, G. Geudtner, and A. M. Koster, First-principle calculations of large fullerenes, *J. Chem. Theory Comput.* **5**, 29 (2009).
- [27] P. W. Dunk, N. K. Kaiser, C. L. Hendrickson, J. P. Quinn, C. P. Ewels, Y. Nakanishi, Y. Sasaki, H. Shinohara, A. G. Marshall, and H. W. Kroto, Closed network growth of fullerenes, *Nat. Commun.* **3**, 855 (2012).
- [28] J. W. Martin, G. J. McIntosh, R. Arul, R. N. Oosterbeek, M. Kraft, and T. Söhnle, Giant fullerene formation through thermal treatment of fullerene soot, *Carbon* **125**, 132 (2017).
- [29] S. Wang, Q. Chang, G. Zhang, F. Li, X. Wang, S. Yang, and S. I. Troyanov, Structural studies of giant empty and endohedral fullerenes, *Front. Chem.* **8**, 607712 (2020).
- [30] E. Ghavanloo, H. Rafii-Tabar, A. Kausar, G. I. Giannopoulos, and S. A. Fazelzadeh, Experimental and computational physics of fullerenes and their nanocomposites: Synthesis, thermo-mechanical characteristics and nanomedicine applications, *Phys. Rep.* **996**, 1 (2023).
- [31] T. D. Donnelly, T. Ditmire, K. Neuman, M. D. Perry, and R. W. Falcone, High-order harmonic generation in atom clusters, *Phys. Rev. Lett.* **76**, 2472 (1996).
- [32] C. Vozzi, M. Nisoli, J. Caumes, G. Sansone, S. Stagira, S. De Silvestri, M. Vecchiocattivi, D. Bassi, M. Pascolini, L. Poletto *et al.*, Cluster effects in high-order harmonics generated by ultrashort light pulses, *Appl. Phys. Lett.* **86**, 111121 (2005).
- [33] O. Smirnova, Y. Mairesse, S. Patchkovskii, N. Dudovich, D. Villeneuve, P. Corkum, and M. Y. Ivanov, High harmonic interferometry of multi-electron dynamics in molecules, *Nature (London)* **460**, 972 (2009).
- [34] S. A. Mikhailov and K. Ziegler, Nonlinear electromagnetic response of graphene: Frequency multiplication and the self-consistent-field effects, *J. Phys.: Condens. Matter* **20**, 384204 (2008).
- [35] H. K. Avetissian, A. K. Avetissian, G. F. Mkrtchian, and K. V. Sedrakian, Creation of particle-hole superposition states in graphene at multiphoton resonant excitation by laser radiation, *Phys. Rev. B* **85**, 115443 (2012).
- [36] H. K. Avetissian, G. F. Mkrtchian, K. G. Batrakov, S. A. Maksimenko, and A. Hoffmann, Multiphoton resonant excitations and high-harmonic generation in bilayer graphene, *Phys. Rev. B* **88**, 165411 (2013).
- [37] P. Bowlan, E. Martinez-Moreno, K. Reimann, T. Elsaesser, and M. Woerner, Ultrafast terahertz response of multilayer graphene in the nonperturbative regime, *Phys. Rev. B* **89**, 041408(R) (2014).
- [38] I. Al-Naib, J. E. Sipe, and M. M. Dignam, High harmonic generation in undoped graphene: Interplay of inter- and intraband dynamics, *Phys. Rev. B* **90**, 245423 (2014).
- [39] L. A. Chizhova, F. Libisch, and J. Burgdörfer, Nonlinear response of graphene to a few-cycle terahertz laser pulse: Role of doping and disorder, *Phys. Rev. B* **94**, 075412 (2016).
- [40] H. K. Avetissian and G. F. Mkrtchian, Coherent nonlinear optical response of graphene in the quantum Hall regime, *Phys. Rev. B* **94**, 045419 (2016).
- [41] D. Dimitrovski, L. B. Madsen, and T. G. Pedersen, High-order harmonic generation from gapped graphene: Perturbative response and transition to nonperturbative regime, *Phys. Rev. B* **95**, 035405 (2017).
- [42] H. K. Avetissian and G. F. Mkrtchian, Impact of electron-electron Coulomb interaction on the high harmonic generation process in graphene, *Phys. Rev. B* **97**, 115454 (2018).
- [43] S. A. Sato, H. Hirori, Y. Sanari, Y. Kanemitsu, and A. Rubio, High-order harmonic generation in graphene: Nonlinear coupling of intraband and interband transitions, *Phys. Rev. B* **103**, L041408 (2021).
- [44] Ó. Zurrón-Cifuentes, R. Boyero-García, C. Hernández-García, A. Picón, and L. Plaja, Optical anisotropy of non-perturbative high-order harmonic generation in gapless graphene, *Opt. Express* **27**, 7776 (2019).
- [45] M. S. Mrudul and G. Dixit, High-harmonic generation from monolayer and bilayer graphene, *Phys. Rev. B* **103**, 094308 (2021).
- [46] Y. Zhang, L. Li, J. Li, T. Huang, P. Lan, and P. Lu, Orientation dependence of high-order harmonic generation in graphene, *Phys. Rev. A* **104**, 033110 (2021).
- [47] F. Dong, Q. Xia, and J. Liu, Ellipticity of the harmonic emission from graphene irradiated by a linearly polarized laser, *Phys. Rev. A* **104**, 033119 (2021).
- [48] H. K. Avetissian, G. F. Mkrtchian, and A. Knorr, Efficient high-harmonic generation in graphene with two-color laser field at orthogonal polarization, *Phys. Rev. B* **105**, 195405 (2022).
- [49] Y. Murakami and M. Schüler, Doping and gap size dependence of high-harmonic generation in graphene: Importance of consistent formulation of light-matter coupling, *Phys. Rev. B* **106**, 035204 (2022).
- [50] T. Tamaya, H. Akiyama, and T. Kato, Shear-strain controlled high-harmonic generation in graphene, *Phys. Rev. B* **107**, L081405 (2023).
- [51] B. Avchyan, A. Ghazaryan, K. Sargsyan, and K. V. Sedrakian, High harmonic generation in triangular graphene quantum dots, *J. Exp. Theor. Phys.* **134**, 125 (2022).
- [52] B. R. Avchyan, A. G. Ghazaryan, S. S. Israelyan, and K. V. Sedrakian, High harmonic generation with many-body Coulomb interaction in rectangular graphene quantum dots of armchair edge, *J. Nanophoton.* **16**, 036001 (2022).
- [53] B. Avchyan, A. Ghazaryan, K. Sargsyan, and K. V. Sedrakian, On laser-induced high-order wave mixing and harmonic generation in a graphene quantum dot, *JETP Lett.* **116**, 428 (2022).
- [54] S. Gnawali, R. Ghimire, K. R. Magar, S. J. Hossaini, and V. Apalkov, Ultrafast electron dynamics of graphene quantum dots: High harmonic generation, *Phys. Rev. B* **106**, 075149 (2022).
- [55] D. Bauer, F. Ceccherini, A. Macchi, and F. Cornolti,  $C_{60}$  in intense femtosecond laser pulses: Nonlinear dipole response and ionization, *Phys. Rev. A* **64**, 063203 (2001).
- [56] G. P. Zhang, Optical high harmonic generation in  $C_{60}$ , *Phys. Rev. Lett.* **95**, 047401 (2005).
- [57] G. P. Zhang and T. F. George, Ellipticity dependence of optical harmonic generation in  $C_{60}$ , *Phys. Rev. A* **74**, 023811 (2006).
- [58] M. F. Ciappina, A. Becker, and A. Jaroń-Becker, High-order harmonic generation in fullerenes with icosahedral symmetry, *Phys. Rev. A* **78**, 063405 (2008).
- [59] R. A. Ganeev, L. B. Elouga Bom, J. Abdul-Hadi, M. C. H. Wong, J. P. Brichta, V. R. Bhardwaj, and T. Ozaki, Higher-order harmonic generation from fullerene by means of the

- plasma harmonic method, *Phys. Rev. Lett.* **102**, 013903 (2009).
- [60] R. A. Ganeev, L. B. Elouga Bom, M. C. H. Wong, J.-P. Brichta, V. R. Bhardwaj, P. V. Redkin, and T. Ozaki, High-order harmonic generation from C<sub>60</sub>-rich plasma, *Phys. Rev. A* **80**, 043808 (2009).
- [61] P. V. Redkin and R. A. Ganeev, Simulation of resonant high-order harmonic generation in a three-dimensional fullerene-like system by means of a multiconfigurational time-dependent Hartree-Fock approach, *Phys. Rev. A* **81**, 063825 (2010).
- [62] T. Topcu, E. A. Bleda, and Z. Altun, Drastically enhanced high-order harmonic generation from endofullerenes, *Phys. Rev. A* **100**, 063421 (2019).
- [63] R. A. Ganeev, C. Hutchison, T. Witting, F. Frank, S. Weber, W. A. Okell, E. Fiordilino, D. Cricchio, F. Persico, A. Zaïr *et al.*, High-order harmonic generation in fullerenes using few- and multi-cycle pulses of different wavelengths, *J. Opt. Soc. Am. B* **30**, 7 (2013).
- [64] G. P. Zhang and Y. H. Bai, High-order harmonic generation in solid C<sub>60</sub>, *Phys. Rev. B* **101**, 081412(R) (2020).
- [65] H. K. Avetissian, A. G. Ghazaryan, and G. F. Mkrtchian, High harmonic generation in fullerene molecules, *Phys. Rev. B* **104**, 125436 (2021).
- [66] H. K. Avetissian, S. Sukiasyan, H. H. Matevosyan, and G. F. Mkrtchian, Disorder-induced effects in high-harmonic generation process in fullerene molecules, *Results Phys.* **53**, 106951 (2023).
- [67] G. Orlando, C.-M. Wang, T.-S. Ho, and S.-I. Chu, High-order harmonic generation in disordered semiconductors, *J. Opt. Soc. Am. B* **35**, 680 (2018).
- [68] C. Yu, K. K. Hansen, and L. B. Madsen, Enhanced high-order harmonic generation in donor-doped band-gap materials, *Phys. Rev. A* **99**, 013435 (2019).
- [69] C. Yu, K. K. Hansen, and L. B. Madsen, High-order harmonic generation in imperfect crystals, *Phys. Rev. A* **99**, 063408 (2019).
- [70] A. Pattanayak, Mrudul M. S., and G. Dixit, Influence of vacancy defects in solid high-order harmonic generation, *Phys. Rev. A* **101**, 013404 (2020).
- [71] H. Irvani, K. K. Hansen, and L. B. Madsen, Effects of vacancies on high-order harmonic generation in a linear chain with band gap, *Phys. Rev. Res.* **2**, 013204 (2020).
- [72] K. Chinzei and T. N. Ikeda, Disorder effects on the origin of high-order harmonic generation in solids, *Phys. Rev. Res.* **2**, 013033 (2020).
- [73] T. Hansen and L. B. Madsen, Doping effects in high-harmonic generation from correlated systems, *Phys. Rev. B* **106**, 235142 (2022).
- [74] C.-L. Xia, J.-Q. Liu, L.-J. Lü, A.-W. Zeng, Z.-L. Li, and X.-B. Bian, Theoretical study of high-order harmonic generation in solutions, *J. Phys. B: At. Mol. Opt. Phys.* **55**, 045401 (2022).
- [75] G. Orlando, M.-I. Lee, and T.-S. Ho, Ellipticity dependence of high-order harmonic generation in disordered semiconductors, *J. Phys. B: At. Mol. Opt. Phys.* **55**, 185601 (2022).
- [76] J. P. Deng, D. D. Ju, G. R. Her, C. Y. Mou, C. J. Chen, Y. Y. Lin, and C. C. Han, Odd-numbered fullerene fragment ions from C<sub>60</sub> oxides, *J. Phys. Chem.* **97**, 11575 (1993).
- [77] F. Banhart, Irradiation effects in carbon nanostructures, *Rep. Prog. Phys.* **62**, 1181 (1999).
- [78] M. Terrones, H. Terrones, F. Banhart, J.-C. Charlier, and P. Ajayan, Coalescence of single-walled carbon nanotubes, *Science* **288**, 1226 (2000).
- [79] R. L. Martin and J. P. Ritchie, Coulomb and exchange interactions in C<sub>60</sub><sup>z-</sup>, *Phys. Rev. B* **48**, 4845 (1993).
- [80] K. Harigaya and S. Abe, Optical-absorption spectra in fullerenes C<sub>60</sub> and C<sub>70</sub>: Effects of Coulomb interactions, lattice fluctuations, and anisotropy, *Phys. Rev. B* **49**, 16746 (1994).
- [81] J.-C. Charlier, J.-P. Michenaud, X. Gonze, and J.-P. Vigneron, Tight-binding model for the electronic properties of simple hexagonal graphite, *Phys. Rev. B* **44**, 13237 (1991).
- [82] M. Yoshida, VRML gallery of fullerenes, <http://www.jcrystal.com/steffenweber/gallery/Fullerenes/Fullerenes.html>.
- [83] A. Gilbert, IQmol molecular viewer, <http://iqmol.org>.
- [84] F. Ding, Theoretical study of the stability of defects in single-walled carbon nanotubes as a function of their distance from the nanotube end, *Phys. Rev. B* **72**, 245409 (2005).
- [85] V. M. Pereira, J. M. B. Lopes dos Santos, and A. H. Castro Neto, Modeling disorder in graphene, *Phys. Rev. B* **77**, 115109 (2008).
- [86] G.-D. Lee, C. Z. Wang, E. Yoon, N.-M. Hwang, D.-Y. Kim, and K. M. Ho, Diffusion, coalescence, and reconstruction of vacancy defects in graphene layers, *Phys. Rev. Lett.* **95**, 205501 (2005).
- [87] K. Ohno, Some remarks on the Pariser-Parr-Pople method, *Theor. Chim. Acta* **2**, 219 (1964).
- [88] K. Harigaya, Effects of Coulomb interaction on the nonlinear optical response in C<sub>60</sub>, C<sub>70</sub>, and higher fullerenes, *J. Phys.: Condens. Matter* **10**, 6845 (1998).
- [89] G. P. Zhang, M. S. Si, M. Murakami, Y. H. Bai, and T. F. George, Generating high-order optical and spin harmonics from ferromagnetic monolayers, *Nat. Commun.* **9**, 3031 (2018).
- [90] S. Larsson, A. Volosov, and A. Rosén, Optical spectrum of the icosahedral C<sub>60</sub>, “follene-60”, *Chem. Phys. Lett.* **137**, 501 (1987).
- [91] M. D. Newton and R. E. Stanton, Stability of buckminsterfullerene and related carbon clusters, *J. Am. Chem. Soc.* **108**, 2469 (1986).
- [92] R. Haddon, L. E. Brus, and K. Raghavachari, Electronic structure and bonding in icosahedral C<sub>60</sub>, *Chem. Phys. Lett.* **125**, 459 (1986).
- [93] J. de Vries, H. Steger, B. Kamke, C. Menzel, B. Weisser, W. Kamke, and I. Hertel, Single-photon ionization of C<sub>60</sub>- and C<sub>70</sub>-fullerene with synchrotron radiation: Determination of the ionization potential of C<sub>60</sub>, *Chem. Phys. Lett.* **188**, 159 (1992).
- [94] T. Koopmans, Über die Zuordnung von Wellenfunktionen und Eigenwerten zu den einzelnen Elektronen eines Atoms, *Physica* **1**, 104 (1934).
- [95] Y.-L. Lin and F. Nori, Electronic structure of single- and multiple-shell carbon fullerenes, *Phys. Rev. B* **49**, 5020 (1994).
- [96] M. Pudlak and R. Pincak, Energy gap between highest occupied molecular orbital and lowest unoccupied molecular orbital in multiwalled fullerenes, *Phys. Rev. A* **79**, 033202 (2009).
- [97] K. Amini, J. Biegert, F. Calegari, A. Chacón, M. F. Ciappina, A. Dauphin, D. K. Efimov, C. F. de Morisson Faria, K. Giergiel, and P. Gniewek, Symphony on strong field approximation, *Rep. Prog. Phys.* **82**, 116001 (2019).

- [98] C. A. Ullrich, *Time-Dependent Density-Functional Theory* (Oxford University Press, Oxford, UK, 2011).
- [99] A. E. Kaplan and P. L. Shkolnikov, Superdressed two-level atom: Very high harmonic generation and multiresonances, *Phys. Rev. A* **49**, 1275 (1994).
- [100] H. K. Avetissian, B. R. Avchyan, and G. F. Mkrtchian, Coherent radiation by two-level quantum systems with permanent dipole moments under multiphoton resonant laser excitation, *J. Phys. B: At., Mol. Opt. Phys.* **45**, 025402 (2012).
- [101] H. K. Avetissian, A. K. Avetissian, B. R. Avchyan, and G. F. Mkrtchian, Wave mixing and high harmonic generation at two-color multiphoton excitation in two-dimensional hexagonal nanostructures, *Phys. Rev. B* **100**, 035434 (2019).